BNL-91408-2010-JA

AUTOMATED RETRIEVALS OF PRECIPITATION PARAMETERS USING NON-RAYLEIGH SCATTERING AT 95-GHZ

Scott E. Giangrande*, Edward P. Luke, and Pavlos Kollias[1]

[1] Department of Atmospheric and Oceanic Sciences, McGill University
* Corresponding author: Scott E. Giangrande, sgrande@bnl.gov

Accepted for publication in
J. Atmos. Oceanic Technol.
(May 2010)

Environmental Sciences Department/Atmospheric Sciences Division

Brookhaven National Laboratory
P.O. Box 5000
Upton, NY 11973-5000
www.bnl.gov

DISCLAIMER

Abstract

Automated retrievals of vertical air motion and drop size distribution (DSD) slope parameter from the surface to the base of the melting layer are presented using a technique for W-band (95-GHz) profiling radars. The technique capitalizes on non-Rayleigh resonance signatures found in the observed Doppler spectra to estimate the mean vertical air motion. The slope parameter of the DSD for an assumed exponential form is retrieved through an inversion of the Doppler spectra. Extended testing is performed in central Oklahoma for a month-long period of observation that includes several midlatitude convective line trailing stratiform events featuring low to moderate rainfall rates (< 1 mm hr^{-1} to 30 mm hr^{-1}). Low-level DSD slope parameter retrievals are shown in agreement (bias of -1.48 cm^{-1} and rms error of 4.38 cm^{-1}) with collocated surface disdrometer DSD observations. Velocity retrievals indicate a net downward motion in stratiform rain of 0.05 ms^{-1} with a standard deviation of 0.24 - 0.3 ms^{-1}. Time-height examples drawn from the available dataset illustrate fine scale structures, as well as evidence of drop sorting due to differential terminal velocity and wind shear.

1. Introduction

Accurate measurements of precipitation are essential in our efforts to understand the connection between atmospheric dynamics and storm microphysics. Traditionally, the most identifiable precipitation measurements from scanning weather radar systems are estimates of the rainfall rate and surface rainfall accumulation. Retrievals of these quantities are undeniably challenging as a consequence of scattering (dependency on the sixth power of the raindrop diameter), radar measurement geometry and several known microphysical limitations (e.g, Sanchez-Diezma et al. 2000; Ryzhkov 2007; Doviak and Zrnic 1993, Sec. 8.4). For a number of applications (e.g., climatology, hydrology), modest instantaneous retrieval errors are acceptable if no long-term bias is introduced. However, detailed process-oriented microphysical studies as well as appropriate characterization of scanning radar measurements (e.g., uncertainty in radar estimates of precipitation) necessitates accurate, high-resolution (space/time) and simultaneous measurements of raindrop size distributions (DSD), vertical air motions, turbulence and environmental parameters.

In a vertically pointing mode, radars provide high-resolution measurements of the vertical structure of precipitation and the recorded Doppler spectra from these systems offers the distribution of the radar return power as a function of the observed Doppler velocity. Several methods have been proposed for the inversion between a recorded Doppler spectrum and the retrieval of a DSD (or cloud drop distributions, e.g., Battan 1964; Atlas et al. 1973; Gossard et al. 1997; Babb et al. 2000; Kollias et al. 2001, 2002). However, uncertainties in the inversion introduced by the contributions of the vertical air

motion to the observed Doppler velocity and Doppler spectra smearing effects as a consequence of turbulence and averaging limit the accuracy of these methods (e.g., Atlas et al. 1973).

Recent studies and the launch of CloudSat that carries the first 94-GHz (λ = 3.2 mm, W-band) radar in space have demonstrated the potential value of traditional 'cloud' radar systems in precipitation (e.g., Stephens et al. 2002; Kollias et al. 2002, 2007a; Matrosov 2005; Haynes et al. 2009; Ellis et al. 2009). Despite fundamental limitations of radar measurements at shorter wavelengths (notably, attenuation in rain), high-resolution cloud radars operating at 94-GHz can help to overcome the deadlock introduced by radar Doppler spectra-based inversion methods for retrieval of the DSD due to the effects of the vertical air motion. Following a technique first introduced by Lhermitte (1988), it is possible to estimate the Doppler shift in response to the vertical air motion and relate the 'quiet air' Doppler velocities in the spectrum to hydrometeor fall velocities. The retrieval technique (briefly described here) capitalizes on the W-band backscattering cross-section as a function of raindrop diameter that oscillates due to non-Rayleigh resonance effects (Mie 1908). The oscillations occur within typical raindrop sizes and, under precipitating conditions, are reflected as patterns of maxima and minima in the observed Doppler spectrum. Since raindrop sizes can be reliably mapped to the associated locations of maxima and minima in the observed Doppler spectrum, accurate retrievals of vertical motion are possible. Previous study has suggested there is no rainfall rate threshold for application of this technique, rather a minimum raindrop size threshold (e.g., Kollias et al. 2002). Although severe attenuation in rain eventually limits the usefulness of W-band radar (e.g., extinction of the signal), velocity retrievals are not immediately tied to the

magnitude (spectral density) of the received signal and therefore viable provided relative minima and maxima are observed.

Well-matched observations of the vertical air motions, raindrop sizes and their fall speeds in two dimensions (time and height) are rare. To date, this resonance-based technique has met with limited application in studies of shallow warm rain (Kollias et al. 1999; 2001), convective (Kollias et al. 2003) and stratiform rain (Firda et al. 1999; Kollias et al. 2002), often in the context of air motion retrievals and simulation-based efforts. In addition to air motion retrievals, this study capitalizes on the accuracy of velocity retrievals for simultaneous retrieval of bulk slope parameter Λ (cm^{-1}) of an exponential DSD. Emphasis has been placed on automated retrieval methods to explore an extended, real-word characterization of W-band retrievals that has not been previously offered in the literature. Establishing connections between W-band radar-based inversions and surface disdrometer platforms are necessary, as all instrument retrievals are impacted by sampling and processing shortcomings (e.g., as in Campos and Zawadzki 2000).

Retrievals in this study utilize the W-band cloud radar (WACR) platform located at the Southern Great Plains (SGP) climate research facility of the Department of Energy's Atmospheric Radiation Measurement (ARM) program in Lamont, OK (e.g., Kollias et al. 2007b). These retrievals are drawn from multiple events collected during a climatological peak of convective, warm season precipitation for the SGP region. The SGP central research facility and surrounding north-central Oklahoma region are heavily instrumented and include operational S-band NEXRAD WSR-88D (KVNX) oversight, simultaneous 35-GHz millimeter MMCR cloud radar measurements and collocated

disdrometer observations available at 1-minute temporal resolution for cross-validation of radar-based DSD slope retrievals. Results and discussion for the cumulative performance and a detailed case study for a widespread precipitation event follow a summary of the available instrumentation and formal outline of the automated retrieval techniques.

2. Instrumentation

a. W-band Cloud Radar

The W-band ARM cloud radar (WACR) is the primary instrument used for precipitation retrievals in this study. A 95-GHz vertically pointing single antenna Doppler radar is housed at the ARM SGP central facility in Lamont, OK. At this very short wavelength ($\lambda \approx 3.2$ mm), the radar is highly sensitive to small liquid droplets and ice crystals (-40 dBZ at 2 km, 1 s dwell).

The WACR utilizes a high pulse repetition frequency (10 kHz) that yields an unambiguous Doppler velocity window of $\pm$ 7.885 ms^{-1}. Current spatial and temporal resolution of the radar data is 43 m vertical and 4.28 s. The 4.28 s temporal resolution accounts for 2.14 s of alternate scanning modes and a 2.14 s temporal scanning window of interest that corresponds to a spectral average of 80 individual 256-point Fast Fourier Transform (FFT) Doppler spectra. The 2 foot antenna of the WACR provides a narrow beamwidth (0.5°) making the radar suitable for the sampling of small atmospheric volumes at close distances in rain.

b. Supplemental Surface Instrumentation

The heavily instrumented SGP central facility and surrounding Oklahoma region offers several options for detailed analysis of precipitation and validation of radar retrievals. A Joss and Waldvogel disdrometer (Model RD-80, manufactured by Disdromet Inc.; Joss and Waldvogel 1967) is collocated with the WACR and serves as the primary source of validation for radar-based DSD slope retrievals. Estimates for the

slope Λ and intercept N_0 parameter of an assumed exponential DSD (e.g., Marshall and Palmer 1948) are routinely calculated by this system at 1-minute accumulation windows.

Complimentary radar observations at two wavelengths less attenuated in precipitation are available from the 35-GHz (Ka-band) MilliMeter Cloud Radar (MMCR, $\lambda \approx 8$ mm) collocated with the WACR and the nearby 3-GHz (S-band) operational NEXRAD WSR-88D ($\lambda \approx 10$ cm) located at Vance AFB (KVNX, approximately 60 km from the ARM field site). A surface meteorological station and routine atmospheric soundings at the ARM field site provide regular measurements of state variables including temperature, pressure, and rainfall accumulation/rate. The ARM suite of instruments also includes a ceilometer and lidar systems that provide valuable information on the location of cloud base.

3. Retrieval Methodology

Resonance effects on the observed W-band Doppler spectrum open several opportunities for the detailed study of precipitation (e.g., Lhermitte 1988). Several studies outline W-band precipitation retrievals (as in Section 3a), therefore emphasis for this section is on the practical implementation and accuracy limitations for long-term automation on the ARM WACR system.

a. Retrieval of Precipitation Parameters at W-band

For a vertically pointing radar system, the spectral density of a given velocity bin is described as

$$S_d(v) = \sigma_b(D)N(D)\frac{dD}{dv}, \quad (1)$$

where N(D) is the number concentration and σ_b(D) is the backscattering cross-section of a raindrop with diameter D and a terminal fall velocity v. Examples of WACR W-band Doppler spectra in the absence of a mean vertical motion are provided in Fig. 1 (solid, noisy lines). Lhermitte (1988) first suggested that the minimum in observed Doppler spectra at W-band closely corresponds to the contribution from raindrops with the diameter of the first resonance minimum in the radar backscattering cross-section (D ~ 1.65 mm). By applying a relationship for raindrop fall speed as a function of diameter (e.g., Gunn and Kinzer 1949), one can accurately determine the terminal fall speed associated with this particular raindrop size. Thus, an estimate of the mean vertical air velocity is revealed through the offset between the terminal velocity for the diameter

associated with the first minimum and the observed velocity of the relative minimum in the observed Doppler spectrum.

A combination of characteristics from observed Doppler spectra is useful to retrieve DSD parameters in precipitation. Slope and shape parameter retrievals from a functional form DSD through inversions of (1) have been suggested at W-band (e.g., Firda et al. 1999; Kollias et al. 2002). Previous work has been on the results of simulations, with less attention to extended surface validation and automated methods noting constraints in data volume and processing. Nevertheless, it is well-understood that Doppler spectra defined by (1) and associated resonance features also respond to bulk changes of N(D). Fig. 1 contains theoretical curves following the expression in (1) with N(D) equal to a constant (dashed lines), the upper dashed curve corresponding to a larger value for N(D) = constant. As an example, for the theoretical curves where N(D) is held constant, spectral density is largely driven by the backscattering cross-section term in (1). Hence, in the simplest case, the location of the first minimum (D_M ~ 1.65 mm), as well as the first and second maxima/peaks (D_1 ~ 1.15 mm and D_2 ~ 2.25 mm, as in Fig. 1, respectively) are reasonably well-known.

Relative differences in the magnitudes of spectral features are tied to the DSD. That is, as a distribution tends toward higher concentrations of smaller droplets, the relative magnitudes and locations of the spectral features will shift. This link is illuminated using an exponential DSD (e.g., Marshall and Palmer 1948) of the form

$$N(D) = N_O e^{-\Lambda D}, \tag{2}$$

where Λ is the slope of the DSD and N_0 is the intercept as before. The inset to Fig. 1 contains spectral density curves for a typical range of Λ values. We note the location of

the first resonance minimum in the Doppler spectra (D_M, v ~ 5.8 m s^{-1}) is well-behaved and does not respond to large-scale changes in Λ (to within 5 cm s^{-1} for exponential-type DSD function). This property of the minimum for exponential-type DSDs helps explain a general usefulness of this feature for accurate velocity retrievals. As expected, the magnitude and locations of the spectral peaks are shown sensitive to bulk slope changes.

b. Automated Retrievals of Precipitation Parameters Using Non-Rayleigh Techniques

i. Spectral Preprocessing and non-Rayleigh Feature Identification

WACR Doppler spectra undergo a spectral averaging of the 80 individual spectra collected over a 2 second window. Preprocessing is required to obtain smooth spectra for better identification of bulk spectral features including the primary minimum. For the Nyquist velocity of the WACR, basic velocity dealiasing is required for typical light/moderate precipitation observations. This is accomplished by shifting spectra such that the left edges of the principle peaks are spaced from the left edges of the FFT arrays by a small predetermined offset. We have selected 30 bins (~1.8 ms^{-1}) as an initial offset. Here, it is noted that the velocity of the principle peak left edge is also viable to determine a cursory starting estimate for the vertical air velocity and applicable for basic self-consistency purposes (assumes small droplets have negligible fall speeds).

After initial processing, a check of the spectral suitability for the techniques is performed. Specifically, resonance-based techniques necessitate the availability of drop sizes sufficiently larger than the diameter of the first non-Rayleigh minimum within the radar resolution volume so as to allow a 'relative' minimum in the Doppler spectrum. In simple terms, one should expect the first resonance valley to be located to the right of the

principle peak left edge V_L, by the terminal fall velocity V_T associated with that resonance drop size. Here, the simplest approach is a width-based screening that rejects all spectra with a principle peak width narrower from the left to right edge than the predicted terminal fall velocity.

Following this basic suitability screening, a second order Gaussian Continuous Wavelet Transform of scale 8 is applied to all remaining spectra (as shown for an example in Fig. 2, dashed line).This serves as a bandpass filter suitably matched to the first minima. The Continuous Wavelet Transform (CWT) has been extensively investigated as a tool for robust detection of relevant transient features, such as peaks and edges, within complicated, noisy signals (e.g., Mallat and Hwang, 1992; Vetterli and Herley, 1992). This method was selected since noisiness and the presence of additional, minor peaks and valleys in the observed spectra could be confusing to other forms of automated detection.

The number of local minima found in the CWT output is counted. The principle peak left and right edge each produce one CWT output minimum of their own (as in Fig 2). Thus, when only two local minima are found, no 'resonance' valleys have been designated within the spectrum and no further processing is performed. If three or more local minima are found in the CWT output (as is the case in Fig. 5), the leftmost and rightmost minima are removed from further consideration, as they are presumed to belong to the principle peak left and right edges. On the remaining CWT output local minima, a test is performed to determine the minima that fall within a predetermined velocity acceptance window. In one implementation of the algorithm, the center position of this velocity acceptance window is offset from the principle peak left edge by an

expected terminal fall velocity, $V_C = V_L + V_T$. The width of this window sets a tolerance range within which the actual air velocity offset may be found. We have used a conservative +/- 70 bins value (or roughly +/- 4.0 m s^{-1}) with success to mitigate large, instantaneous errors (> 1 m/s). The velocity acceptance window is adaptable, however wider windows (e.g., allowing minima to be detected at values smaller than 4 m s^{-1}) will increase the probability of incorrect feature detection, particularly when the liquid assumption is no longer valid. For example, melting snow mixed with liquid precipitation within the melting layer will often exhibit secondary peak/valleys of prominence at slower spectral fall velocities and techniques are generally not as straightforward or recommended well within a mixed-phase layer.

For all local CWT minima within the acceptance window, the lowest (i.e., strongest) is identified and the position is an estimate of the first resonance valley. This estimate can still deviate by several velocity bins from the position of the corresponding local minimum in the original Doppler spectrum. A further refinement is attempted by searching the original spectrum for a lower spectral density value within a small neighborhood (e.g., +/- 3 bins) surrounding the CWT valley velocity estimate (e.g., following Lhermitte 2002). Note, it is possible that a spectrum contains no relative minima to the right edge of the spectrum. In these situations, retrievals are not attempted.

ii. Spectral Alignment (Shifting) and Additional Considerations

Mean air velocity and DSD parameter retrievals necessitate proper spectral alignment according to an accurate droplet size - fall velocity relationship. Following

Lhermitte (1988), the terminal fall speed relation for raindrops assumes an exponential fit to Gunn and Kinzer (1949) observations (Herein, GK)

$$V_o = 9.25 * [1 - \exp(-6.8D^2 - 4.88D)], \quad (3)$$

where D is in [cm] and V in [ms^{-1}]. The stated accuracy of (3) is to within 3 cm s^{-1} of the GK observations between 0.5 and 6 mm.

The reference diameter of the first minimum in the radar backscattering cross-section at W-band is D ~ 1.65 mm and translates to a fall velocity from (3) of ~5.8 ms^{-1}. Since the GK measurements are valid for a particular set of still air surface conditions, adjustments for changes in air density are required. A correction following Foote and duToit (1969) is applied of the form

$$\frac{V_z}{V_o} = \left(\frac{\rho_o}{\rho_z} \right)^n \quad (4)$$

where ρ is the air density at altitude (z) and surface (o) levels. Here, the coefficient n in (4) is a function of the raindrop diameter of interest (e.g., Beard 1985) and set to n = 0.5 specific for the D ~ 1.65 mm drop size in following Lhermitte (2002).

Scattering computations from the T-Matrix approach (e.g., Mishchenko 2000) are used to calculate radar backscattering cross-section values specific for the 95 GHz WACR system. Backscattering cross-section computations depend on several factors including raindrop temperature and shape, as noted by several authors (e.g., Lhermitte 1988; Aydin and Lure 1991; Firda et al. 1999). Raindrop shapes following the axis ratio expression from Brandes et al. (2002) are used for calculations in this study.

Air density and T-Matrix scattering computations imply regular ingest of atmospheric state variables. Collocated ARM surface instrumentation and regular

atmospheric radiosondes (launched at 6 hour intervals) provide the necessary thermodynamic profiles and melting layer cut-offs. To improve temporal consistency, ARM Merged Sounding products (a blend of available ARM and other available radiosondes assimilated with surface observations and various short-term model output) are incorporated at high temporal resolution to better match the temporal sampling of the WACR. Each ARM Merged Sounding is associated with a fractional value indicating radiosonde/model contribution to the merged product.

c. Applicability and Error Characterization of WACR Automated Techniques

It is important to consider system-based limitations and shortcomings of the automated retrievals for proper comparisons with surface instruments and modeling/precipitation efforts. For the SGP WACR retrieval dataset (Table 1), nearly all (>95%) Doppler spectra collected to 1 km AGL associated with a non-zero surface rainfall rate were suitable for retrievals, indicating the presence of suitable-sized drops for resonance signatures within precipitation sampling volumes. The opportunity to perform retrievals to a typical base of the melting layer (~2.5 km) was high, often with at least 70% of a column from the surface to the base of the melting layer containing viable spectra (>90% for 1 mm hr^{-1} < rainfall rate < 10 mm hr^{-1} and ~70% for higher surface rainfall rates where attenuation in rain limits retrievals with height). The bulk of the retrieval hours (~94% of 35,000+ instantaneous retrievals at the lowest gate) were performed for surface rainfall rates < 10 mm hr^{-1}.

Retrievals of vertical air motions capitalizing on resonance features have been previously reported accurate to within 10 cm s^{-1} and shown insensitive to a wide range of

turbulence intensity parameterizations (e.g., Firda et al. 1999; Kollias et al. 2002; Lhermitte 2002). Accuracy claims are based on the testing of simulated spectra over an extensive range of input DSD parameters and parameterizations for noise and Gaussian-form subvolume turbulence. Of interest is a weak relationship between the location of the first resonance minimum and the bulk slope of the DSD (as in Fig. 1, to within 5 cm s^{-1} for an exponential form with $0 < \Lambda < 65$ cm^{-1}). Specific to the WACR, a constraint is imposed by the resolution of the Doppler spectrum ($\Delta v \sim 6$ cm s^{-1}), which is coarser than the reported accuracy under most simulated conditions. Testing of the CWT method revealed detected minima typically to within a single misplacement of a velocity bin ($\Delta v \sim 10$ cm s^{-1}). A pronounced presence/absence of particular drop sizes in response to isolated-intense drop sorting (e.g., along strong updraft/downdraft interface) or melting particles could also obscure prominent spectral features. Efforts to ensure the consistency of CWT minima with corresponding spectral features (left edge offset check, spacing relative to predicted peak locations) mitigate gross errors, however limited instantaneous misplacements on the order of a few spectral bins are unavoidable.

Beyond these considerations, the accuracy of velocity retrievals is mapped to an assumed fall speed relation and corrections at altitude. GK measurements do not describe precipitating conditions and limited references exist for fall speeds at altitude (e.g., Lhermitte 2002). From (3) and (4), modest air density variability within precipitation can impact retrieval accuracy through the estimates of fall speed velocities to the same order as the stated retrieval accuracy (~10 cm s^{-1}). The combined uncertainty in placement and fall speed mapping may argue for a more conservative stance on velocity retrieval accuracy in operational settings than previously reported, perhaps to within 10-20 cm s^{-1}.

Slope parameter retrieval accuracy is challenging as this is coupled with velocity retrievals and methods for 'fitting' an assumed DSD form (system/retrieval noise). Previous simulation studies using traditional exponential and gamma forms report an accuracy of W-band inversion methods typically to within 3 cm^{-1} of simulated inputs provided spectral noisiness and turbulence do not obscure prominent spectral features (e.g., Kollias et al. 2002). Inversion techniques following (1) also imply sampling errors within small and large drop regimes as computational limitations, for example as in the consequence of a rapidly increasing dD/dV term at larger sizes.

To offer a different perspective on retrieval errors, this study explores the automated retrieval performance through comparisons with collocated surface disdrometer observations performing a similar parameter fit. Here, we perform an exponential slope parameter fit using nontruncated estimates of the 3^{rd} and 6^{th} moments (e.g., Waldvogel 1974), similar to the ARM reference Joss-Waldvogel disdrometer standard calculation. These efforts offer an initial reference for WACR retrievals against a familiar standard. The subject of a more appropriate or optimal slope parameter fit for validation, especially as it pertains to known disdrometer instrument limitations for sampling of small and large drops, is not well-resolved (e.g., Smith 2003; Smith et al. 2009). Retrieval intercomparison and expectations therein are also clouded by similar temporal and spatial sampling limitations of platforms (e.g., Zawadzki 1975; Campos and Zawadzki 2000). Additional factors including noisiness as a consequence of variability within a physical process (sorting effects, as described for Joss-Waldvogel 1-minute disdrometer efforts; Lee and Zawadzki 2005), will introduce additional uncertainty between the 'instantaneous' retrievals from both platforms.

4. Automated Retrieval Observations from May/June 2007

As listed in Table 1, the events from May and early June 2007 were selected to assess automated retrieval performance covering a total of 14 cases and 85 hours of measurable precipitation recorded by the WACR system. Many events featured extended observations in isolated convective systems, as well as classical MCS squall-line convective storms followed by extended trailing stratiform regions. As a consequence of severe attenuation in rain, WACR retrievals through the strongest precipitation cores are often limited to within 1.5 km AGL. As described in the previous section, the bulk of the retrieval hours are associated with lower surface rainfall rates and stratiform regions trailing strong convective lines. Cumulative statistics for these events are offered, as well as a case-study from the May 1st 2007 event for a detailed look at the automated retrieval fields.

a. Cumulative Automated Retrievals, Velocity

For each W-band range-gate, instantaneous retrievals are conducted without any information from surrounding gates (independent) and exhibit high spatial correlations in time-height with adjacent retrievals (~0.8). Instantaneous vertical velocity measurements (convention is positive - downward) predominantly range from ±3.0 ms^{-1}, within kinematic definitions of bulk stratiform precipitation found in the literature (e.g., Yuter and House 1995ab). Approximately 5% of the instantaneous velocity retrievals for the events exhibited magnitudes greater than 1 ms^{-1}. Fig. 3 (top) shows a cumulative two dimensional histogram (height and velocity CFAD, e.g., Yuter and Houze 1995ab) for

velocity retrievals with rainfall rate > 1 mm hr^{-1} and radiosonde fractions greater than 50% (indicative that ingest sounding data reasonably-matched in time with the observations). The bulk of retrievals in Fig. 3 (top) are obtained in lower rainfall rates, exhibiting a downward net air motion profile beneath the melting layer (downward offset ~ 0.04 ms^{-1}). The bulk of observations are between ±0.3 ms^{-1} with a standard deviation of 0.24 ms^{-1}. As the quality of velocity retrievals are potentially linked to factors including regime (concatenation of convective and stratiform events) and sounding viability, we have isolated retrievals for only lower rainfall rates < 2 mm hr^{-1} and at the times of highest radiosonde fraction (>90%) to approximate well-observed, light widespread precipitation conditions (Fig. 3, bottom). For this subset, the CFAD reveals similar net downward motion and overall standard deviation as before (0.05 ms^{-1} and 0.3 ms^{-1}, respectively).

b. Cumulative Radar – Disdrometer Slope Parameter Comparisons

Slope retrievals for the lowest available range gate from the W-band radar (300 m AGL) are compared with measurements from the collocated surface disdrometer (Fig. 4). For the scatterplot in Fig. 4 (~24,000 instantaneous radar observations with rain rate > 1 mm hr^{-1}), radar-based 'instantaneous' slope retrievals are paired with the closest matched 'instantaneous' 1-minute disdrometer estimate. Although instantaneous retrieval comparisons assume system, spatial and temporal mismatch, the results demonstrate a mean bias of -1.48 cm^{-1} (radar underestimation) and an rms error of 4.36 cm^{-1}. Similar bias and rms errors were observed for rain rate thresholding of > 2 mm hr^{-1} (-1.38 cm^{-1} and 4.26 cm^{-1} for 16,500+ points not shown, respectively). Instantaneous radar slope

retrievals as a function of surface rainfall rate indicate slope measurement variability decreases at higher rainfall rates and associated with lower slopes (Fig. 5). Instantaneous retrievals fall within expectations for Λ-R model relations following the N_0 value of Marshall-Palmer ($N_0 = 0.08$ cm^{-4}, dashed line) and bounded by a spread of light rain and 'thunderstorm' conditions ($N_0 = 0.3$ cm^{-4} and $N_0 = 0.014$ cm^{-4}, top and bottom solid lines, respectively; following Lhermitte 2002). A decreasing correlation is also noted between time series of slope retrievals performed at a surface reference height to those performed immediately aloft (Fig. 6). These observations provide an indication for the consistency of these independent instantaneous retrievals from one gate to the next, but also the variability (sorting effects) of the DSD slope parameter with height.

c. Example Observations of a 1 May 2007 Storm

During the early overnight hours through mid-afternoon of May 1st 2007, an upper level low pressure system tracked from west Texas through the state of Oklahoma. Favorable thermodynamic conditions in the region contributed to widespread cloud cover and precipitation development over the ARM central facility in Lamont. Initial precipitation was in the form of light, stratiform rain (rain rate ~ 1-3 mm hr^{-1}) developing in advance of the center of low pressure or surface boundary. Moderate precipitation rates (rain rates > 10 mm hr^{-1}) were recorded as the center of the low approached the field site. The strongest precipitation band to pass over the field site is associated with a weak segment of a developing convective line.

Time-height plots of the equivalent radar reflectivity factor Ze for the May 1st 2007 event are provided for three radar systems (KVNX, WACR and MMCR) in Fig. 7.

S-band reflectivity measurements as from KVNX are well-associated with the changes in precipitation-sized particles and precipitation intensity (e.g., Doviak and Zrnic 1993). Although attenuation in rain is negligible at S-band, fine-scale insight from KVNX in its current operational mode is limited by the coarse resolution volume (~ 1 km^3 at 50 km), beam broadening, SNR thresholds and the effect of Earth curvature. Nevertheless, these measurements provide context for several situations for which cloud radar systems are heavily attenuated in rain and therefore unavailable to higher altitudes.

The precipitation as viewed by surveillance radar matches several classic 'stratiform' characteristics from the literature (e.g., Steiner et al. 1995). A 'bright band' signature is observed around 3.3 km throughout most of the event, in agreement with freezing level heights recorded by radiosondes regularly launched at the ARM facility. The bright band enhancement is observed at S-band and an isolated enhancement is also visible for this event in MMCR Ka-band measurements that are sensitive to select precipitation-sized melting particles. Although a pronounced enhancement is not apparent in WACR measurements, Doppler spectra multi-modality features infer some presence of melting snowflakes down to heights of 2.5-2.8 km (e.g., bottom of the melting layer, not shown). KVNX Ze measurements at low levels are in agreement with field site observations of light/moderate rainfall rates between 1 to 5 mm hr^{-1}. A weak convective line (Ze ~ 45 dBZ) forms over the site after 1800 UTC and surface observations indicate a shift to moderate/heavy rainfall rates of 10-30 mm hr^{-1}. The increase in the precipitation intensity may also be inferred from cloud radar Ze measurements that exhibit severe bias due to attenuation in rain and are unavailable above 2 km during the most intense convective cells.

Hourly time-height cross-sections of retrieval segments of vertical velocity and slope parameter as in Figs. 8 (1300-1400 UTC) and 9 (1815-1915 UTC) also match with the expectations based on larger-scale event features. Slope parameter retrievals trend with large-scale changes in the precipitation patterns as inferred by the reflectivity factor fields at the multiple wavelengths. For example, lowest values of slope often correspond to extended regions beneath pronounced 'bright band' enhancements that are most likely associated with the presence of additional and larger melting particles (sizes that the current methodology of slope retrieval is most sensitive).

A closer inspection of retrieved precipitation fields of air velocity and slope reveal fine scale structures. It is quite common to observe small, but intense embedded structures a few hundred meters in depth with periods of oscillation on the order of 1-2 minutes. Slope retrievals feature trails or 'streaks' of Λ in time/height. Most often, slope parameter signatures are consistent with large particles originating from the melting of large snow aggregates reaching the surface first due to the differential fall speed of raindrops. Retrievals performed near the end of the event (Fig. 9) reveal pronounced structures in time-height. These structures possibly indicate isolated regions of strong horizontal wind shear, waves, and additional size sorting of the largest particles.

Slope retrievals for the lowest available range gate from the W-band radar (solid black lines) are compared with measurements obtained from the collocated surface disdrometer (solid blue line) in Figs. 8,9 (bottom panels). The rainfall rate observed by the disdrometer during the 1-minute collection period has been included on the images for an additional reference (solid green line). The temporal sampling of the instruments has been taken into account and radar-based retrievals have been smoothed in time to

better match 1-minute disdrometer sampling and mitigate 'instantaneous' instrument scatter as was observed in Fig. 4. For this event, the mean bias (radar – disdrometer) is again near -1.0 cm^{-1} .

5. Discussion and Conclusions

This study demonstrates the applicability of an automated, 94-GHz radar Doppler spectra-based technique for the retrieval of precipitation parameters in low to moderate rainfall rates (1 – 30 mm hr^{-1}). In a vertically pointing mode, the techniques is performed for range gates where the radar signal in not fully attenuated in rain and requires the presence of particular sized raindrops within the resolution volume. When these conditions are satisfied, the methods have been automated and are of use for detailed retrieval of vertical air motions and inversions of the Doppler spectra for simultaneous information on the slope of the DSD in the time and height. It is suggested that techniques require minimal signal processing using a continuous wavelet transform methodology for location of relative features in the Doppler spectra. This automation is important if one considers the long-term ARM program plans to deploy W-band systems at all ARM climate research facilities. For this validation effort, known surface instrument limitations motivated the selection of exponential DSD fitting for the intercomparison. However, the authors do not exclude investigations of gamma or other retrievals parameters (including at altitude) provided capable surface disdrometer instruments are collocated.

Results for the month-long application indicate viable retrievals in the Oklahoma warm season for a wide range of rainfall rates (e.g., Kollias et al. 2002). For the SGP dataset, retrievals are demonstrated viable to heavy surface rainfall rates, as in the case-study event recorded near 1834 and 1847 UTC (15 - 30 mm hr^{-1}). It is noted that less than 6% of the valid retrievals for the SGP May 2007 dataset were obtained for rainfall rates

in excess of 10 mm hr^{-1}. During these intense precipitation intervals, retrievals are only available from the surface to heights below 2 km AGL before the beam is attenuated in rain. Retrievals performed during moderate surface rainfall rates < 10 mm hr^{-1} are typically available from the surface to the base of the melting layer or slightly above. Retrieval availability may not project similarly to other precipitation regimes with an absence of moderate drop sizes.

Long-term averages and frequency histograms of velocity retrievals fall within expected ranges for central Oklahoma weak convective and stratiform-type systems. This includes air motion averages in stratiform precipitation that feature a net downward air motion of 0.05 cm s^{-1} and a standard deviation of 25-30 cm s^{-1}. High temporal/spatial resolution plots of retrievals from automated techniques also reveal several complex structures in precipitation fields. Retrieved velocity patterns exhibit various scales of motion embedded within the precipitation field to scales of a few hundred meters and a few minutes in time. Instantaneous air motions are recorded with magnitudes to 3 ms^{-1}, with 5% of the observations exceeding 1 ms^{-1}.

Within this study, it was suggested that poorly-matched environmental soundings carry the potential to introduce significant retrieval bias. An advantage of the ARM climate research facility for W-band retrievals is in an availability of sounding launches and merged model-sounding products at high temporal resolution that lessens these sorts of biases. CFAD segregation revealed only subtle differences in cumulative statistics for retrievals that included possibly lesser-matched ARM merged sounding products. However, as radiosonde launches are often aborted in heavier precipitation and/or launched in advance of oncoming systems, even frequent air density profile availability

may not best represent the environment and occasionally introduce detrimental biases for individual event studies. Merged soundings products are also not immune in situations with model failure to capture initiating or ongoing precipitation.

Long-track slope retrievals at low levels are in agreement with surface disdrometer measurements and error characteristics are in line with statements in the existing literature for W-band retrievals. Known system limitations of the Joss-Waldvogel disdrometer and spatial/temporal retrieval mismatch including physical process noise/sorting effects may help explain additional bias and spread of instantaneous slope retrievals (e.g., Sheppard and Joe 1994; Tokay et al. 2001; Campos and Zawadzki 2000; Lee and Zawadzki 2005). In general, an undersampling of small and larger particles by the impact disdrometer is consistent with the reported offset (bulk radar underestimation, as in Fig. 4) between surface disdrometer observations and the inversion-based radar retrievals following a method of 3^{rd} and 6^{th} moments. That is, WACR-based retrievals feature a larger sampling volume more sensitive to the presence of low concentration larger drops. It is suggested small raindrops are also better sampled by the WACR as compared with the impact disdrometer platform. This disdrometer sampling limitation is consistent with a reversal of the slope retrieval offset (overestimation) at higher values of slope.

Collocation of W-band systems can serve as a strong complement to various ground-based radar and profiler measurements. W-band systems could be a valuable tool for validation of other forms of radar-based wind retrieval and improving our understanding of precipitation processes with appropriate averaging. Here, interpretation of offered 'instantaneous' retrievals of the slope parameter may be suitable within a

remote sensing context, analogous to median-large drop sensitivity of polarimetric differential reflectivity factor ZDR and extend toward exporation on small-scale DSD variability on polarimetric measurements (e.g., Miriovsky et al., 2004). Note, slope parameter retrieval is representative of the particles present in the illuminated volume (weighted toward the contribution of larger drop sizes according to the method of moments), but not relevant for tracing the paths traversed by all particles contributing to that volume. Averaging in time and height is necessary for microphysical insight into various physical processes (as with the 1-minute disdrometer observations; Lee and Zawadzki 2005).

In conjunction with the techniques presented in this study, reflectivity factor from an unattenuated wavelength can be exploited for the retrieval of the intercept parameter N_0 for the assumed DSD. The intercept is estimated by inverting the Rayleigh reflectivity factor formula

$$Z_{UA} = N_O \int_0^\infty D^6 e^{-\Lambda D} dD, \tag{5}$$

where Λ has been obtained for an exponential DSD using W-band retrieval methods. For this study, the operational S-band KVNX system was unaffected by attenuation, but the resolution volume was considered too coarse for an optimal demonstration.

Acknowledgements

Support for this research was funded by the Office of Biological and Environmental Research, Environmental Sciences Division of the U.S. Department of Energy as part of the Atmospheric Radiation Measurement program (Grant No. DE-FG02-08ER64573). The authors would also like to thank Isztar Zawadzki, Frederick Fabry and Mark Berenguer of McGill University for helpful discussions, as well as the anonymous reviewers who have greatly improved the quality of this manuscript.

References

Atlas, D., R. C. Srivastava, and R. S. Sekhon (1973), Doppler Radar Characteristics of Precipitation at Vertical Incidence, *Rev. Geophys.*, 11(1), 1–35.

Aydin, K. and Y. M. Lure, "Millimeter Wave Scattering and Propagation in Rain: A Computational Study at 94 and 140 GHz for Oblate Spheroidal and Spherical Raindrops," IEEE Trans. Geoscience and Remote Sensing, vol. GE-29, 593-601, 1991.

Babb, D.M., J. Verlinde, and B.W. Rust, 2000: The Removal of Turbulent Broadening in Radar Doppler Spectra Using Linear Inversion with Double-Sided Constraints. *J. Atmos. Oceanic Technol.*, **17**, 1583–1595.

Battan, L. J., 1964: Some Observations of Vertical Velocities and Precipitation Sizes in a Thunderstorm. *J. Appl. Meteor.,* **3,** 415–420.

Brandes, E.A., G. Zhang, and J. Vivekanandan, 2002: Experiments in Rainfall Estimation with a Polarimetric Radar in a Subtropical Environment. *J. Appl. Meteor.*, **41**, 674–685.

Beard, K.V., 1985: Simple Altitude Adjustments to Raindrop Velocities for Doppler Radar Analysis. *J. Atmos. Oceanic Technol.*, **2**, 468–471.

Campos, E., and I. Zawadzki, 2000: Instrumental Uncertainties in *Z–R* Relations. , **39**, 1088–1102.

Doviak R. J., and D. S. Zrnić, 1993: *Doppler Radar and Weather Observations*. 2d ed. Academic Press, 562 pp.

Ellis, T. D., T. L'Ecuyer, J. M. Haynes, and G. L. Stephens (2009), How often does it rain over the global oceans? The perspective from CloudSat, *Geophys. Res. Lett.*, 36, L03815, doi:10.1029/2008GL036728.

Firda, J.M., S.M. Sekelsky, and R.E. McIntosh, 1999: Application of Dual-Frequency Millimeter-Wave Doppler Spectra for the Retrieval of Drop Size Distributions and Vertical Air Motion in Rain. *J. Atmos. Oceanic Technol.*, **16**, 216–236.

Foote, G.B., and P.S. Du Toit, 1969: Terminal Velocity of Raindrops Aloft. *J. Appl. Meteor.*, **8**, 249–253.

Gossard, E.E., J.B. Snider, E.E. Clothiaux, B. Martner, J.S. Gibson, R.A. Kropfli, and A.S. Frisch, 1997: The Potential of 8-mm Radars for Remotely Sensing Cloud Drop Size Distributions. *J. Atmos. Oceanic Technol.*, **14**, 76–87.

Gunn, R., and G.D. Kinzer, 1949: The Terminal Velocity of Fall for Water Droplets in Stagnant Air. *J. Atmos. Sci.*, **6**, 243–248.

Haynes, J. M., T. S. L'Ecuyer, G. L. Stephens, S. D. Miller, C. Mitrescu, N. B. Wood, and S. Tanelli (2009), Rainfall retrieval over the ocean with spaceborne W-band radar, *J. Geophys. Res.*, 114, D00A22, doi:10.1029/2008JD009973.

Joss, J., and A. Waldvogel, 1967: A Raindrop Spectrograph with Automatic Analysis. *Pure Appl. Geophys*., **68**, 240-246.

Kollias, P., R. Lhermitte, and B. A. Albrecht, 1999: Vertical Air Motion and Raindrop Size Distributions in Convective Systems Using a 94 GHz Radar. *Geophys. Res. Lett.,* **26,** 3109–3112.

----------, B. A. Albrecht, and F. Marks Jr., 2001: Raindrop sorting induced by convective updrafts. *Geophys. Res. Lett.*, 28(14), 2787–2790.

----------, ----------, and ----------, 2002: Why Mie? *Bull. Amer. Meteor. Soc.*, **83**, 1471–1483.

----------, ----------, and ----------, 2003: Cloud Radar Observations of Vertical Drafts and Microphysics in Convective Rain. *J. Geophys. Res.,* **108,** 4053, doi:10.1029/2001JD002033.

----------, E.E. Clothiaux, M.A. Miller, B.A. Albrecht, G.L. Stephens, and T.P. Ackerman, 2007a: Millimeter-Wavelength Radars: New Frontier in Atmospheric Cloud and Precipitation Research. *Bull. Amer. Meteor. Soc.*, **88**, 1608–1624.

----------, E.E. Clothiaux, M.A. Miller, E.P. Luke, K.L. Johnson, K.P. Moran, K.B. Widener, and B.A. Albrecht, 2007b: The Atmospheric Radiation Measurement Program Cloud Profiling Radars: Second-Generation Sampling Strategies, Processing, and Cloud Data Products. *J. Atmos. Oceanic Technol.*, **24**, 1199–1214.

Lee, G., and I. Zawadzki, 2005: Variability of Drop Size Distributions: Time-Scale Dependence of the Variability and Its Effects on Rain Estimation. *J. Appl. Meteor.*, **44**, 241–255.

Lhermitte, R., 1987: A 94-GHz Doppler Radar for Cloud Observations. *J. Atmos. Oceanic Technol.,* **4,** 36–48.

----------, 1988: Observations of Rain at Vertical Incidence with a 94 GHz Doppler Radar: An Insight of Mie Scattering. *Geophys. Res. Lett.,* **15,** 1125–1128.

Lhermitte, 2002 Centimeter & Millimeter Wavelength Radars in Meteorology, ***Lhermitte Publications***, p. 500

.

Mallat, S.; Hwang, W.L.,1992: "Singularity Detection and Processing with Wavelets," *IEEE Transactions on Information Theory*, vol.38, no.2, pp.617-643.

Marshall, J., and W.M. Palmer, 1948: The Distribution of Raindrops with Size. *J. Atmos. Sci.*, **5**, 165–166.

Matrosov, S.Y., 2005: Attenuation-Based Estimates of Rainfall Rates Aloft with Vertically Pointing K_a-Band Radars. *J. Atmos. Oceanic Technol.*, **22**, 43–54.

Mie, G., 1908: Beitrage zur Optic truber Medien, speziell kolloidaler Metallosungen. *Ann. Phys.,* **30,** 377–442.

Miriovsky, B.J., A.A. Bradley, W.E. Eichinger, W.F. Krajewski, A. Kruger, B.R. Nelson, J.D. Creutin, J.M. Lapetite, G.W. Lee, I. Zawadzki, and F.L. Ogden, 2004: An Experimental Study of Small-Scale Variability of Radar Reflectivity Using Disdrometer Observations, **43,** 106-118.

Mishchenko M. I., 2000: Calculation of the Amplitude Matrix for a Nonspherical Particle in a Fixed Orientation. *Appl. Opt*, **39**, 1026–1031.

Ryzhkov, A.V, 2007: The impact of beam broadening on the quality of radar polarimetric data. *J. Atmos. Oceanic Technol.*, 24, 729–744.

Sanchez-Diezma R., I. Zawadzki, and D. Sempere-Torres, 2000: Identification of the bright band through the analysis of volumetric radar data. *J. Geophys. Res*, 105, 2225–2236.

Sheppard, B., and P. Joe, 1994: Comparison of Raindrop Size Distribution Measurements by a Joss-Waldvogel Disdrometer, a PMS 2DG Spectrometer, and a POSS Doppler Radar. *J. Atmos. Oceanic Technol.*, **11**, 874–887.

Smith, P.L., 2003: Raindrop Size Distributions: Exponential or Gamma—Does the Difference Matter? *J. Appl. Meteor.*, **42**, 1031–1034.

Smith, P.L., D.V. Kliche, and R. W. Johnson, 2009: The Bias and Error in Moment Estimators for Parameters of Drop-Size Distribution Functions: Sampling from Gamma Distributions. *J. Appl. Meteor. Climotol.*, Online Early Release. DOI: 10.1175/2009JAMC2114.1

Steiner, M., R.A. Houze, and S.E. Yuter, 1995: Climatological Characterization of Three-Dimensional Storm Structure from Operational Radar and Rain Gauge Data. *J. Appl. Meteor.*, **34**, 1978–2007.

Stephens, G.L., D.G. Vane, R.J. Boain, G.G. Mace, K. Sassen, Z. Wang, A.J. Illingworth, E.J. O'Connor, W.B. Rossow, S.L. Durden, S.D. Miller, R.T. Austin, A.

Benedetti, C. Mitrescu, and T. CloudSat Science Team, 2002: THE CLOUDSAT MISSION AND THE A-TRAIN. *Bull. Amer. Meteor. Soc.*, **83**, 1771–1790.

Tokay, A., A. Kruger, and W.F. Krajewski, 2001: Comparison of Drop Size Distribution Measurements by Impact and Optical Disdrometers. *J. Appl. Meteor.*, **40**, 2083–2097.

Vetterli, M.; Herley, C., 1992: "Wavelets and Filter Banks: Theory and Design," *IEEE Transactions on Signal Processing*, vol.40, no.9, pp. 2207-2232.

Waldvogel, A., 1974: The N_0 Jump of Raindrop Spectra. *J. Atmos. Sci.*, **31**, 1067–1078.

Yuter, S.E., and R.A. Houze, 1995a: Three-dimensional Kinematic and Microphysical Evolution of Florida Cumulonimbus. Part I: Spatial Distribution of Updrafts, Downdrafts, and Precipitation. *Mon. Wea. Rev.*, **123**, 1921–1940.

Yuter, S. E. and R. A. Houze, Jr., 1995b: Three-dimensional kinematic and microphysical evolution of Florida cumulonimbus. Part II: Frequency distributions of vertical velocity, reflectivity and differential reflectivity. Mon. Wea. Rev., **123**, 1941-1963.

Zawadzki, I.I., 1975: On Radar-Raingage Comparison. *J. Appl. Meteor.*, **14**, 1430–1436.

Figure Captions

Fig. 1: Examples of Doppler spectra from the ARM WACR W-band cloud radar. The Doppler spectra were collected at the same altitude and 3 minutes apart (thick and thin solid lines). Spectral density curves for N(D) = constant are shown for two different constant values (dashed lines). The inset contains spectral density curves for an exponential distribution using different values of the slope parameter (in cm^{-1}). The diameters associated with the first two resonance maxima (D_1 and D_2) as well as the first minimum (D_M) are plotted as reference.

Fig. 2: Example of an observed Doppler spectrum (solid line) and its continuous wavelet transform performed at a scale of 8 (thick dashed line). Locations of the peaks and first minimum are denoted by dotted vertical lines.

Fig. 3: (Top) Cumulative Frequency with Altitude Display (CFAD) of radar-based velocity retrievals for all events and rainfall rates > 1 mm hr^{-1} and radionsonde fraction > 50% (positive – downward). (Bottom) CFAD for retrievals over surface rainfall rates < 2 mm hr^{-1} with radiosonde fraction > 90%.

Fig. 4: Scatterplot of radar-based slope retrievals versus disdrometer slope estimates for SGP May 2007.

Fig. 5: Scatterplot of radar-based slope retrievals versus disdrometer rainfall rate estimates for SGP May 2007. Solid lines represents model slope-rainfall rate curve for a light rain and 'thunderstorm' N_0 = 0.3(top), 0.014(bottom) cm^{-4}, respectively, and dashed line is a model curve for the Marshall-Palmer N_0 = 0.08 cm^{-4}.

Fig. 6: Correlation of radar-based slope retrieval time series as a function of the distance from a surface reference height.

Fig. 7: Time-height mapping of the reflectivity factor at 3-GHz (top), 95-GHz (middle), and 35-GHz (bottom) for the 1 May, 2007 event.

Fig. 8: Precipitation parameter retrievals for the time frame between 1300 UTC and 1400 UTC and (bottom) the time series of observed (disdrometer) and radar-retrieved slope Λ for the same time interval (velocity is positive – downward). Black line is the radar-based retrieval, solid blue line is the 1-minute disdrometer measurements. Green line indicates the rainfall rate observed by the disdrometer.

Fig. 9: As in Fig. 8, but for the time interval between 1815 UTC and 1915 UTC.

Table Caption

Table 1: Listing of SGP events and the hours of observation.

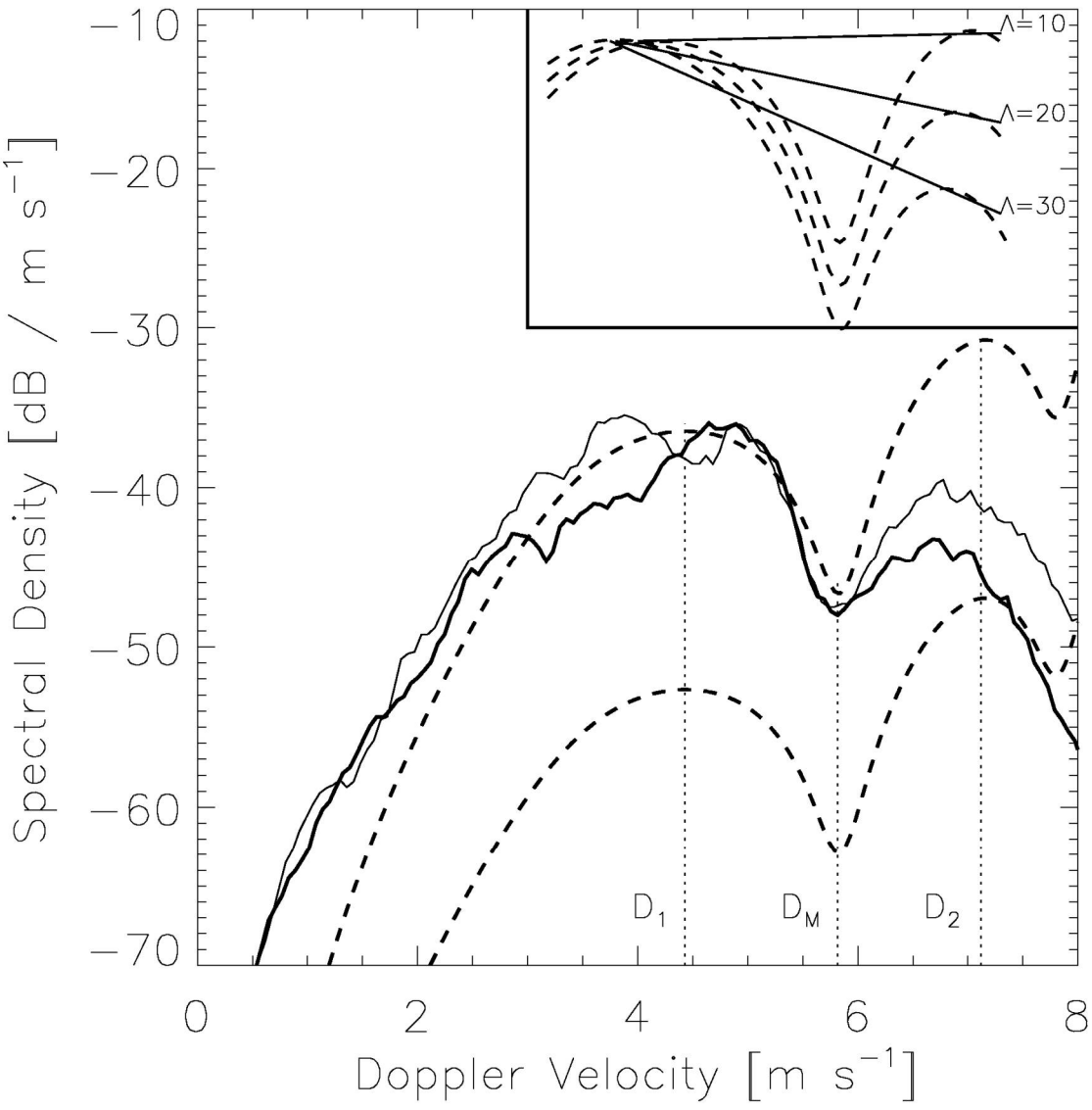

Fig. 1: Examples of Doppler spectra from the ARM WACR W-band cloud radar. The Doppler spectra were collected at the same altitude and 3 minutes apart (thick and thin solid lines). Spectral density curves for N(D) = constant are shown for two different constant values (dashed lines). The inset contains spectral density curves for an exponential distribution using different values of the slope parameter (in cm^{-1}). The diameters associated with the first two resonance maxima (D_1 and D_2) as well as the first minimum (D_M) are plotted as reference.

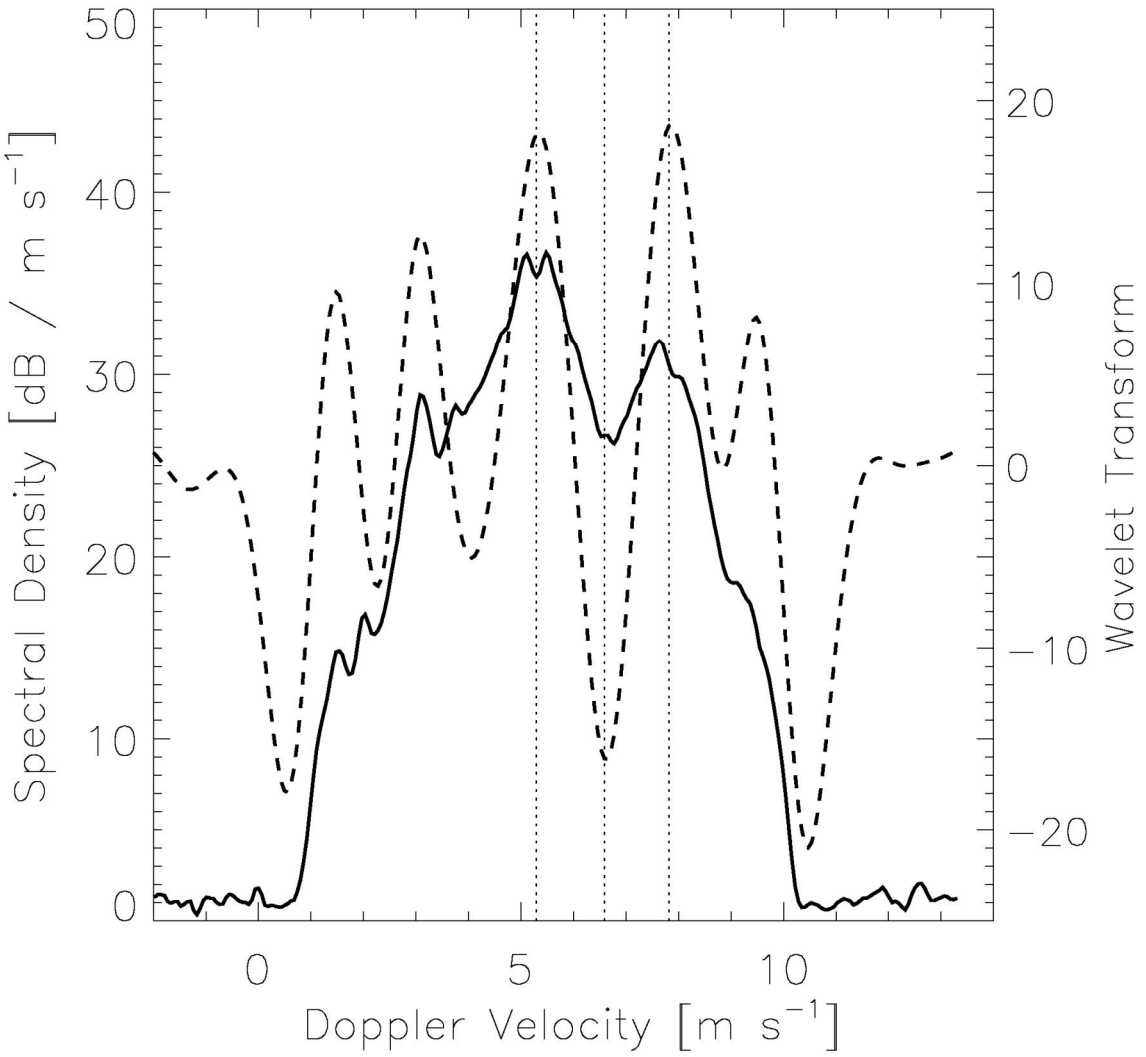

Fig. 2: Example of an observed Doppler spectrum (solid line) and its continuous wavelet transform performed at a scale of 8 (thick dashed line). Locations of the peaks and first minimum are denoted by dotted vertical lines.

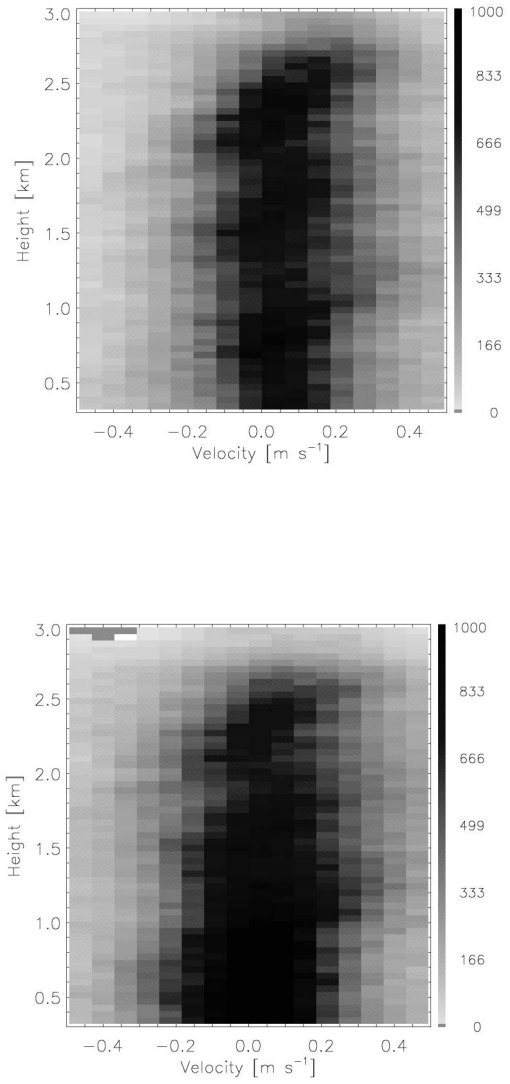

Fig. 3: (Top) Cumulative Frequency with Altitude Display (CFAD) of radar-based velocity retrievals for all events and rainfall rates > 1 mm hr^{-1} and radionsonde fraction > 50% (positive – downward). (Bottom) CFAD for retrievals over surface rainfall rates < 2 mm hr^{-1} with radiosonde fraction > 90%.

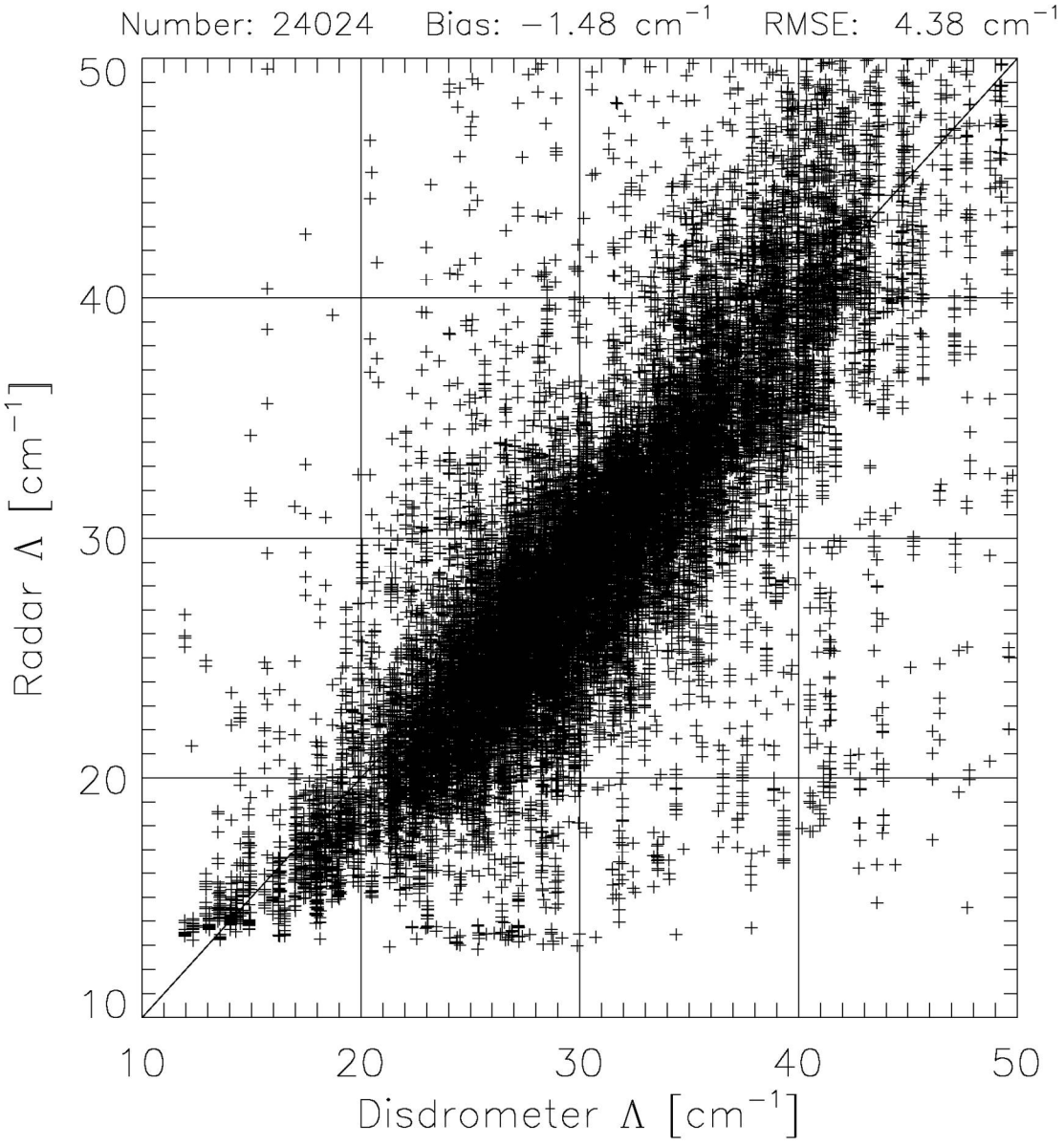

Fig. 4: Scatterplot of radar-based slope retrievals versus disdrometer slope estimates for SGP May 2007.

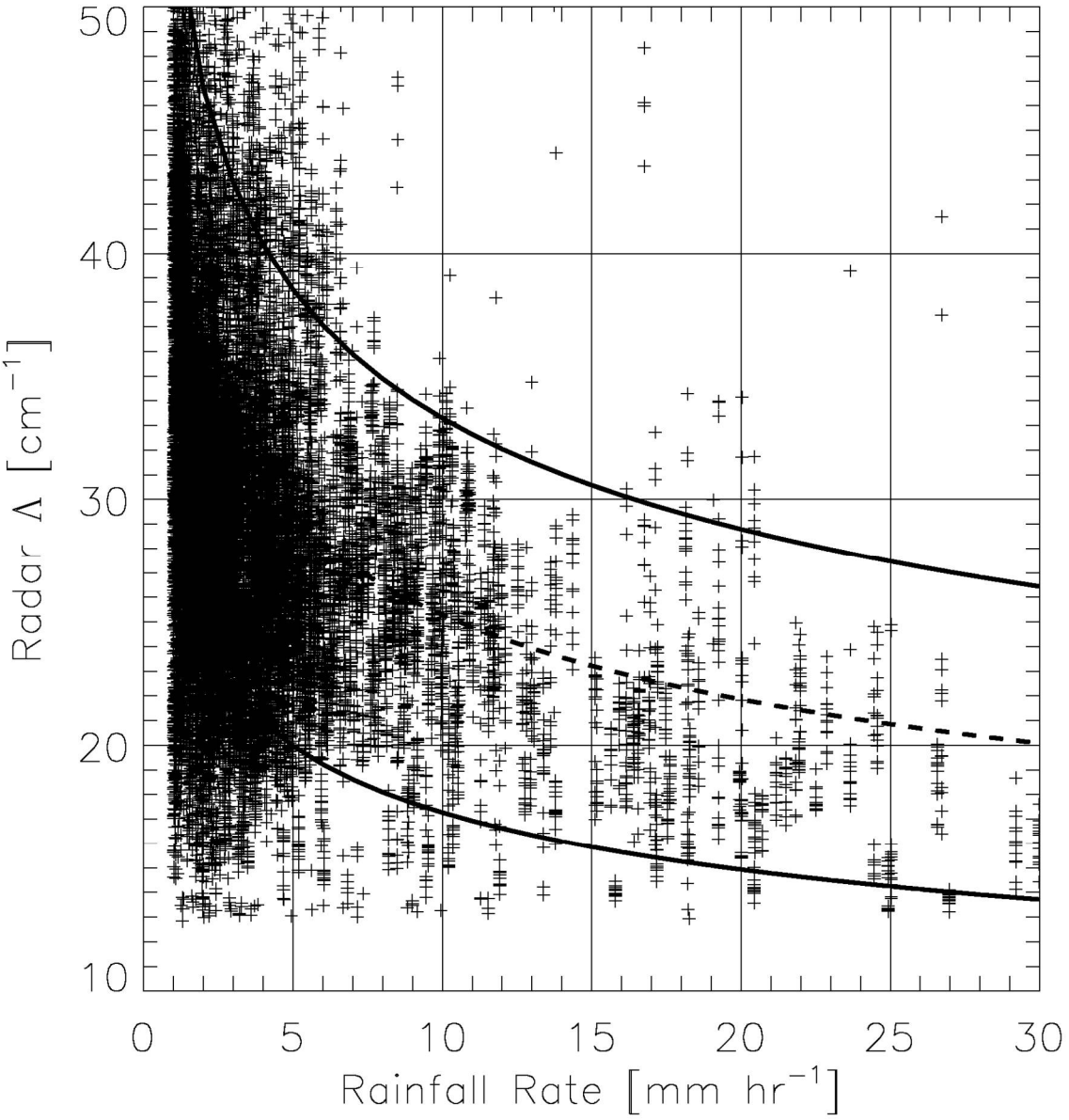

Fig. 5: Scatterplot of radar-based slope retrievals versus disdrometer rainfall rate estimates for SGP May 2007. Solid lines represents model slope-rainfall rate curve for a light rain and 'thunderstorm' N_0 = 0.3(top), 0.014(bottom) cm^{-4}, respectively, and dashed line is a model curve for the Marshall-Palmer N_0 = 0.08 cm^{-4}.

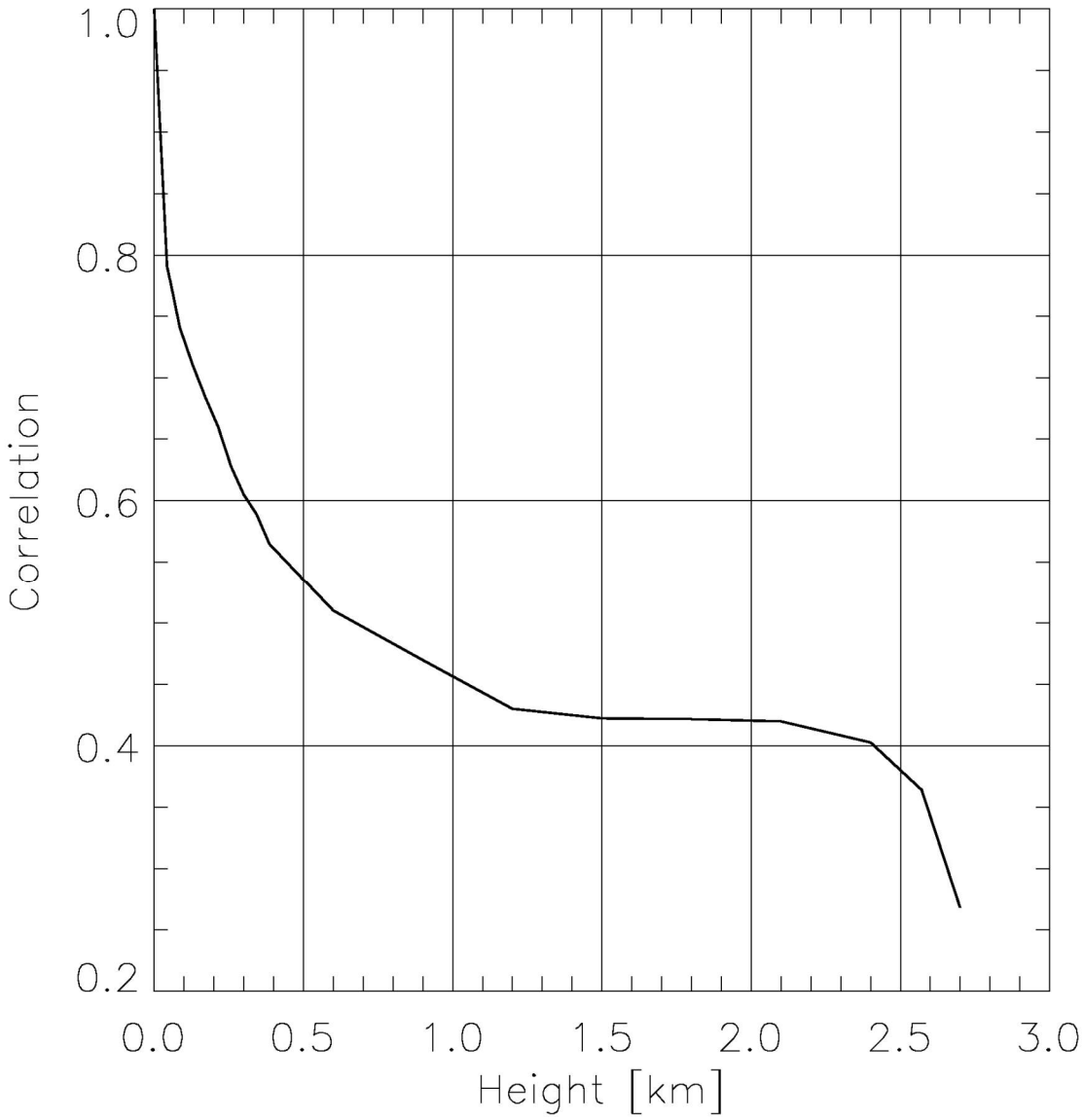

Fig. 6: Correlation of radar-based slope retrieval time series as a function of the distance from a surface reference height.

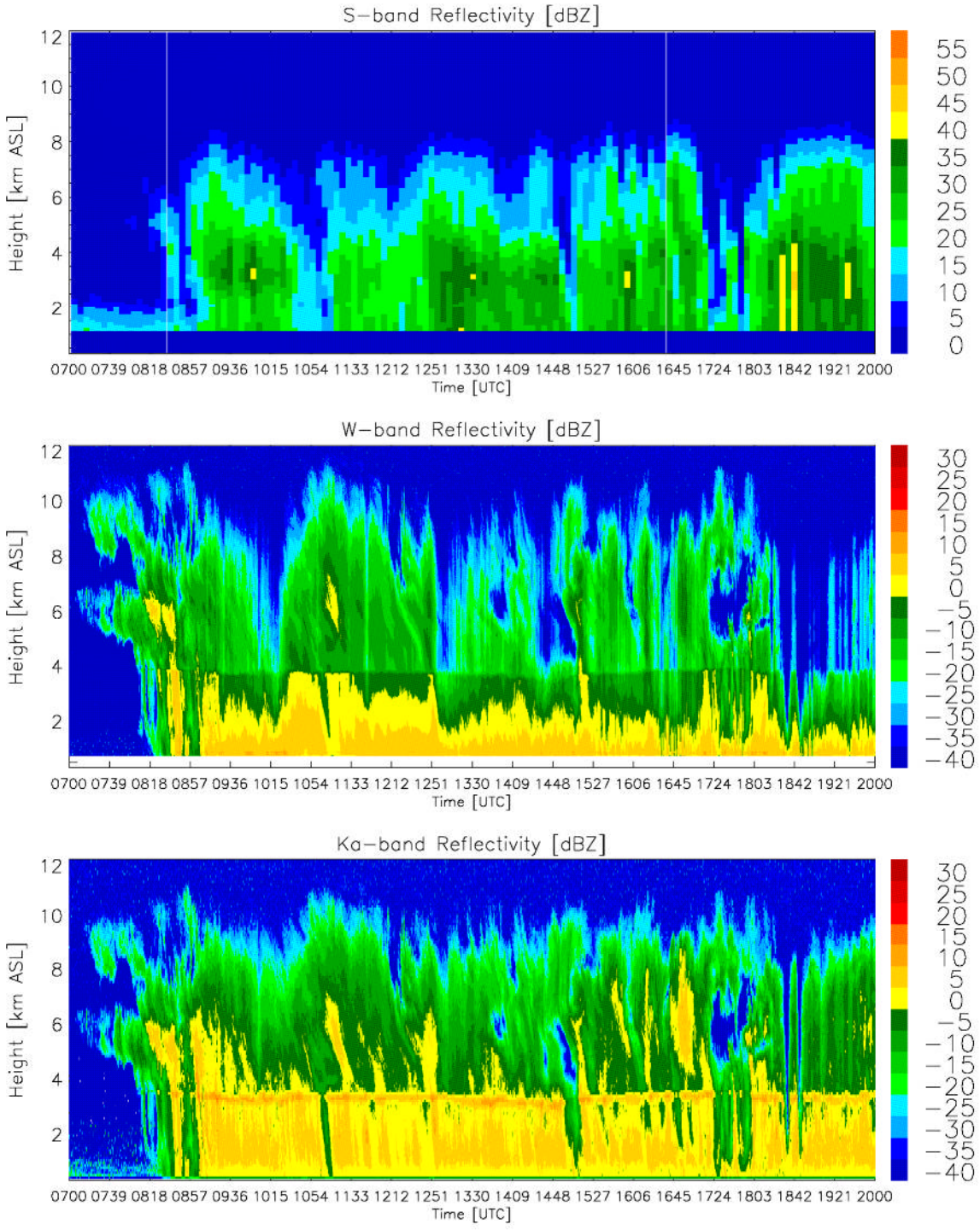

Fig. 7: Time-height mapping of the reflectivity at 3-GHz (top), 95-GHz (middle), and 35-GHz (bottom) for the 1 May, 2007 event.

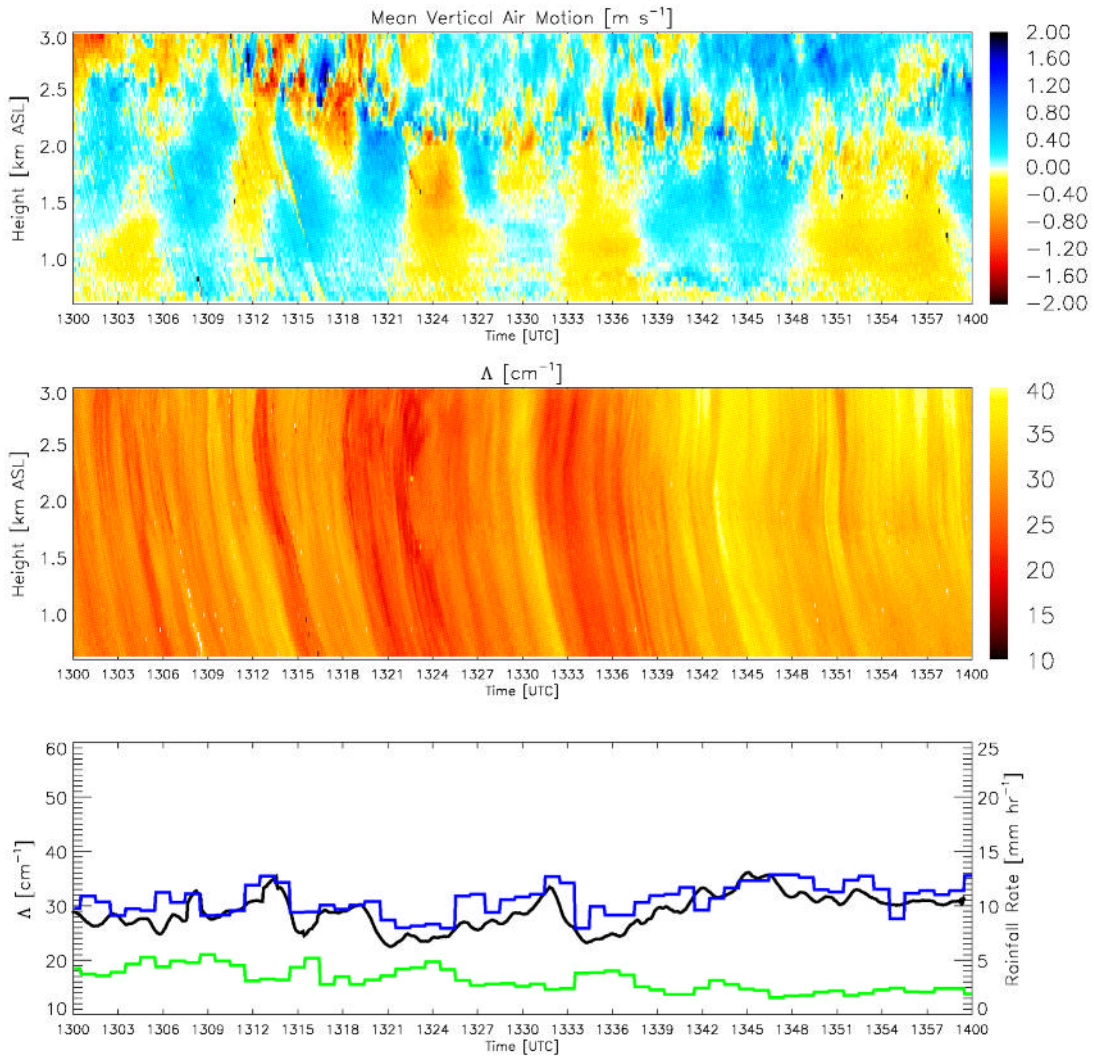

Fig. 8: Precipitation parameter retrievals for the time frame between 1300 UTC and 1400 UTC and (bottom) the time series of observed (disdrometer) and radar-retrieved slope Λ for the same time interval (velocity is positive – downward). Black line is the radar-based retrieval, solid blue line is the 1-minute disdrometer measurements. Green line indicates the rainfall rate observed by the disdrometer.

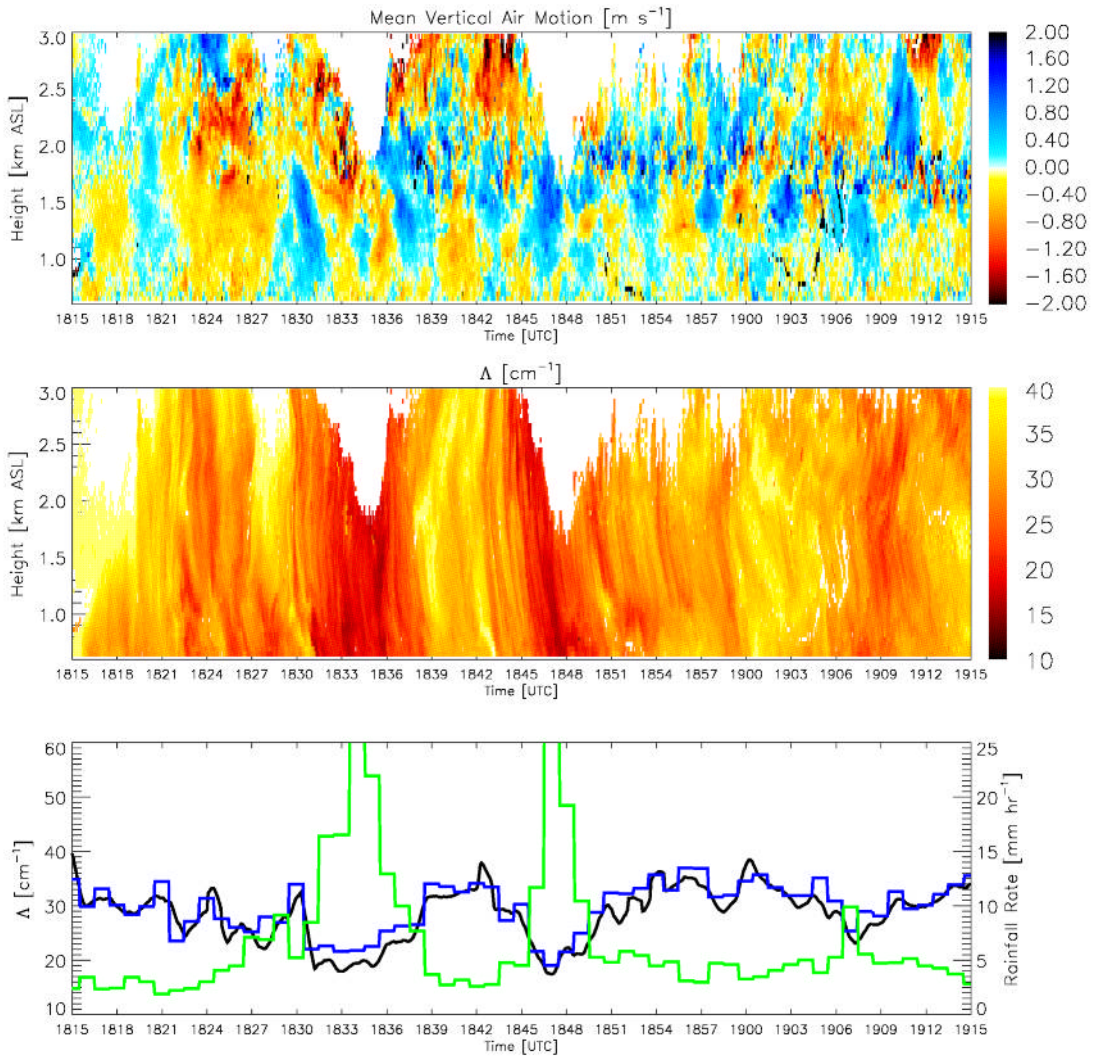

Fig. 9: As in Fig. 8, but for the time interval between 1815 UTC and 1915 UTC.

Table 1: Listing of SGP events and the hours of observation.

Number	Date	Hours (UTC)	Event Type
1.	05/01/07	8 – 22	Weak Convective
2.	05/02/07	18 – 20	Weak Convective
3.	05/03/07	18 – 20	Weak Convective
4.	05/07/07	5 – 13	MCS/trailing stratiform
5.	05/08/07	8, 10-20	MCS/trailing stratiform
6.	05/09/07	4 – 8	MCS/trailing stratiform
7.	05/10/07	13 – 14	Weak Isolated Convective
8.	05/22/07	14 – 15	Weak Stratiform
9.	05/24/07	9 – 13	MCS/trailing stratiform
10.	05/27/07	15 – 22	Convective / Stratiform
11.	05/28/07	00 – 01	Isolated Convective
12.	05/30/07	11 – 14	MCS/trailing stratiform
13.	06/01/07	4 – 12, 21 – 23	MCS/trailing stratiform
14.	06/02/07	00 – 02	Isolated Convective